IEEE Access
Multidisciplinary ⋮ Rapid Review ⋮ Open Access Journal

Received June 22, 2021, accepted August 18, 2021, date of publication August 25, 2021, date of current version September 2, 2021.

Digital Object Identifier 10.1109/ACCESS.2021.3107345

The Sensitivity of Grid-Connected Synchronverters With Respect to Measurement Errors

ZEEV KUSTANOVICH[1], FLORIAN REISSNER[2], SHIVPRASAD SHIVRATRI[2], AND GEORGE WEISS[2]

[1]Israel Electricity Company, North District, Haifa, Israel
[2]School of Electrical Engineering, Tel Aviv University, Ramat Aviv 69978, Israel

Corresponding author: Zeev Kustanovich (kustanz875@gmail.com)

This work was supported in part by Israeli Ministry of Infrastructure, Energy and Water under Grant 217-11-037 and Grant 219-11-128, and in part by the ITN Network WinGrid through the European Union's Horizon 2020 Research and Innovation Program by Marie Sklodowska-Curie under Grant 861398.

ABSTRACT The synchronverter algorithm is a way to control a switched mode power converter that connects a DC energy source to the AC power grid. The main features of this algorithm are frequency and voltage droops as well as synthetic inertia, so that the inverter resembles a synchronous generator (SG). Many versions of this algorithm have been proposed and tested, but all share the same ''basic control algorithm'', which is based on the equations of a SG. We analyze the sensitivity of the output currents of a synchronverter, with respect to the measurement errors. We show that some of the sensitivity functions exhibit high gains at the relevant frequencies, leading to distorted grid currents, which makes the use of this inverter control algorithm problematic. We then do a similar analysis assuming that we have controlled current sources available at the grid output of the converter, that we control using virtual currents generated in the algorithm. The virtual currents are flowing through virtual output inductors, that we can choose to be significantly larger than the actual output inductors. We show that using the current sources reduces the sensitivity considerably, thus indicating a better approach to synchronverter design.

INDEX TERMS Inverter, inertia, Park transformation, synchronverter, virtual synchronous machine, frequency droop, voltage droop, virtual impedance, current control.

I. INTRODUCTION

The shift of the power grid towards distributed generation raises serious questions about the stability and robustness of a grid where most of the power comes from inverters. Most researchers seem to agree that the future inverters must inherit some features of synchronous generator and their prime movers, such as frequency and voltage droops and inertia, see for instance [1]–[3], [5], [8], [9], [11], [19], [23], [28], [30], [34]. One way to meet this demand are synchronverters, introduced in [35], and further developed in [2], [6], [7], [9], [10], [20], [22], [24], [25], [27]–[29], [31]–[33] and several other references.

The hardware of a synchronverter is the same as for a conventional three phase inverter, except that some DC energy storage is required to emulate inertia. This extra storage is normally provided by capacitors or batteries. The novelty lies in the control algorithm, which is based on the (simplified) model of a synchronous generator (SG). In some respects synchronverters are even better for the stability of the grid than SGs, because their parameters are adjustable and they can react faster to changes on the grid.

This paper investigates two related topics: (1) The sensitivity of the currents of a synchronverter functioning according to the basic synchronverter algorithm, when connected to a powerful grid modeled as an infinite bus, with respect to voltage and current measurement errors. (2) The same sensitivity, when the synchronverter works with a virtual output impedance, and the resulting virtual output currents are used as reference signals for ideal current sources injecting currents into the grid. We show that the sensitivities are much reduced in the second case, and hence we suggest that future developments should follow this road.

The associate editor coordinating the review of this manuscript and approving it for publication was Derek Abbott.

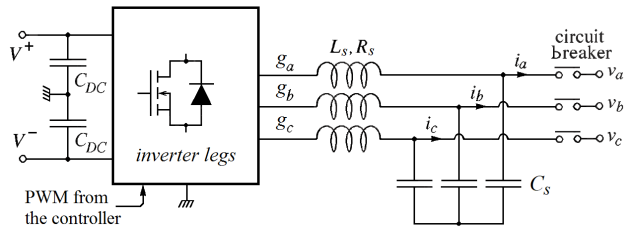

FIGURE 1. An inverter with an LC filter receiving DC voltages V^+, V^- and connected to the AC grid with voltages v_a, v_b and v_c.

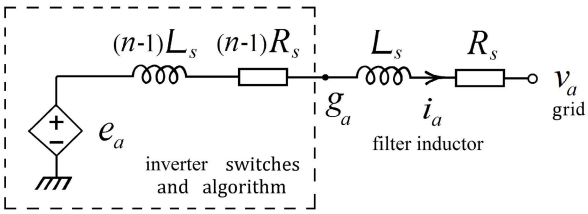

FIGURE 2. The output circuit of a synchronverter with filter inductor L_s and its resistance R_s. e_a is the synchronous internal voltage. The output filter elements multiplied with $(n-1)$ are virtual. Only phase a is shown.

To deal with these aims, we recall the fifth order grid-connected synchronverter model, that takes into account the measurement errors, a variation of the model in our recent paper [16], where the measurement errors are ignored. The equilibrium points of the resulting system are of course the same as for the model in [16], as discussed there. For the sensitivity analysis, we do a small signal analysis around the stable equilibrium points of this model.

For the proper operation of an individual inverter we need the sensitivity of the inverter currents with respect to grid voltage and current measurement errors to be small. Our research is motivated by the following practical observation: in a synchronverter running under the basic algorithm from [35] or one of its later variations, such as the one in [20], the errors can be very disturbing, causing strong distortions of the grid currents, especially at relatively low power. This issue has been pointed out also in our recent conference paper [26], however no detailed analysis has been provided.

To understand intuitively where the problem lies with the synchronverter designs from [20], [34], [35], we look at the simplified circuit diagram of a grid-connected inverter in Figure 1, taken from [16]. The outputs of the algorithm are the desired averages (over one switching cycle) of the voltages g_a, g_b and g_c at the output of the inverter legs. In the original algorithm from [35], g_a, g_b and g_c are the internal synchronous voltages of the virtual SG, while in the version of [20] they are the voltages after the virtual inductor, which is $(n-1)$ times the output filter inductor, as shown in Figure 2 (taken from [20]). (In this paper we do not consider the virtual series capacitor introduced in [20], which is very large so that it has an influence only near the frequency zero.) Thus, the original algorithm is a particular case of the one in [20], corresponding to $n = 1$, and here we consider the version with arbitrary $n \geq 1$ for greater generality. The reasons for increasing the output impedance of the inverter using virtual inductors and virtual resistors have been explained in [20], [21]. In short, the inverter with the classical synchronverter algorithm would be unstable with the very small values of L_s and R_s that are usually found in commercial inverters, and increasing the real filter inductor by a factor of about 30 would make it very bulky and expensive.

A voltage measurement error Δv_a in phase a may be due to a combination of sensor imprecision, calibration errors, quantization errors, and processing delay. This error will cause a similar sized error Δg_a in the signal g_a, because g_a is approximately following v_a. This will cause an error current Δi_a that, expressed via its Laplace transform $\widehat{\Delta i_a}$, is given by:

$$\widehat{\Delta i_a}(s) = \frac{1}{L_s s + R_s}\widehat{\Delta g_a}(s).$$

For a typical inverter of 10 kW nominal output, L_s would be around 2 mH, resulting in an impedance of around 0.63Ω at the nominal grid frequency of 50 Hz. Hence, having Δg_a of the order of 4 V (which is a normal value according to our experience, and is a small error when expressed as a percentage of the AC voltage range) will result in Δi_a of the order of 6 A, which is intolerably high. One can try to fight this phenomenon by striving for very high precision in measurements and calibrations, and devising all sorts of ingenious ways to compensate for the processing delay. However, overall this is a losing battle, and this has led us to seek a fundamentally different approach.

Very briefly, the new approach is to add current loops to the inverter, let the synchronverter work with virtual currents, which results in a very robust system, and then use the virtual currents as reference values for the current loops. If the current loops are good, they can be regarded, at least for low frequencies (hundreds of Hz), as controlled current sources. As already mentioned, we do the sensitivity analysis both for the algorithm from [20], [35] and also for this new approach when we have current sources at the output of the inverter, to understand whether this reduces the sensitivity of the currents with respect to measurement errors. It will turn out that indeed, the sensitivity will be reduced by a large factor, approximately $n - 1$.

The fifth order mathematical model of the grid connected synchronverter containing the measurement errors is derived in Section II. In Section III we briefly recall the main results on the equilibrium points and the stability of this model, derived in our recent paper [16]. In Section IV we perform a small signal analysis around the stable equilibrium points, and we provide Bode plots of the resulting sensitivities, for a typical 10kW inverter. These plots confirm what we have said about sensitivities in this section. In Section V we derive the model and the sensitivities of synchronverters with ideal current sources at their outputs, and we plot these sensitivities for synchronverters with the same parameters as in the example in Section IV. The comparison will show that indeed the current sources lead to a significant improvement.

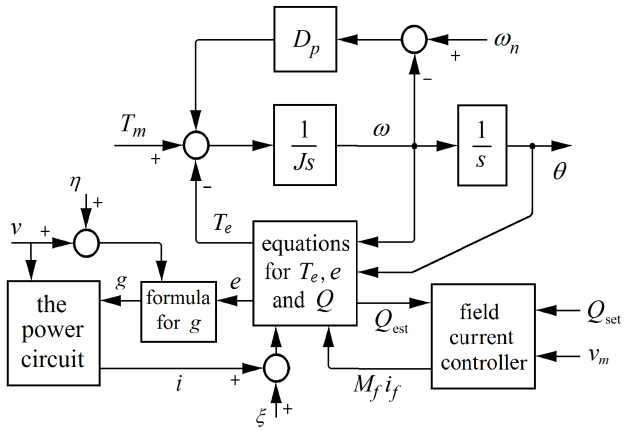

FIGURE 3. The simplified block diagram of a synchronverter with measurement errors, adapted from Figure 2 in [20].

II. MODELLING THE GRID-CONNECTED SYNCHRONVERTER WITH MEASUREMENT ERRORS

In this section we review the basic fifth order model of a synchronverter connected to a sinusoidal, balanced grid with very low impedance, known as an "infinite bus". This model is based on those in [16], [20], [35], which in turn are based on the equations of a SG, as found for instance in [12], [13]. The novelty here is that we also include the influence of the grid voltage and output current measurement errors. We follow the terminology and notation of [16]. The simplified model of a synchronverter, given in Figure 3, shows how the voltage measurement errors η and the current measurement errors ξ influence the signals in a synchronverter. The model ignores low-pass filters included in the algorithm to reduce high frequency noise, as well as saturation blocks included in the algorithm for stability and protection (see [6], [20]).

Let θ_g denote the grid angle and ω_g the grid frequency, so that $\omega_g = \dot{\theta}_g$. The nominal grid frequency is denoted by ω_n. Let θ denote the synchronverter rotor angle, and ω its angular velocity, so that $\omega = \dot{\theta}$. The difference $\delta = \theta - \theta_g$ is the *power angle*. Then the grid voltage vector is

$$v = \sqrt{\frac{2}{3}} V \left[\sin\theta \ \sin\left(\theta - \frac{2\pi}{3}\right) \ \sin\left(\theta + \frac{2\pi}{3}\right) \right]^\top, \quad (1)$$

where V is the rms value of the line voltage.

Denote by $M_f > 0$ the peak mutual inductance between the virtual rotor winding and any one stator winding, by i_f the variable *field current* (or rotor current) and by e the vector of electromotive forces, also called the *internal synchronous voltage*. We rewrite [35, eq.(4)]:

$$e = M_f i_f \omega \left[\sin\theta \ \sin\left(\theta - \frac{2\pi}{3}\right) \ \sin\left(\theta + \frac{2\pi}{3}\right) \right]^\top. \quad (2)$$

We apply the unitary *Park transformation* $U(\theta)$ to (1) and (2). For any three dimensional signal v, the first two components of $U(\theta)v$ are called the dq coordinates of v, denoted by v_d, v_q. By using the notation $m = \sqrt{3/2} M_f$, we obtain

$$v_d = -V \sin\delta, \quad v_q = -V\cos\delta, \quad (3)$$
$$e_d = 0, \quad e_q = -m i_f \omega. \quad (4)$$

The voltage sensors measure v_a, v_b and v_c, while the current sensors are placed to measure i_{ga}, i_{gb} and i_{gc}, in order to avoid most of the switching noise. From the measurements, i_a, i_b and i_c must be estimated, by adding to i_{ga}, i_{gb}, i_{gc} the currents flowing to the filter capacitors (see Figure 1).

Denote by $\eta = [\eta_d \ \eta_q]^\top$ the voltage measurement errors, and by $\xi = [\xi_d \ \xi_q]^\top$ the current measurement errors, expressed in dq coordinates. Thus, the synchronverter control algorithm gets $[(v_d+\eta_d)\,(v_q+\eta_q)]^\top$ as grid voltage measurements in dq coordinates. Similarly, $[(i_d+\xi_d)\,(i_q+\xi_q)]^\top$ are the estimated synchronverter output currents, expressed in dq coordinates.

We have already introduced the voltages $g = [g_a \ g_b \ g_c]^\top$ that the synchronverter algorithm sends to the PWM block. Note that the basic algorithm is a special case of the one presented below, corresponding to $n = 1$. In the basic synchronverter algorithm, we have $g = e$. According to the modified synchronverter equations [20, eq.(22)] and taking into account the measurement errors, we have

$$g_d = \frac{(n-1)(v_d+\eta_d)+e_d}{n}, \ g_q = \frac{(n-1)(v_q+\eta_q)+e_q}{n}.$$

By applying the Park transformation on the circuit equations corresponding to Figure 2, we have

$$L_s \frac{di_d}{dt} = -R_s i_d + \omega L_s i_q + g_d - v_d, \quad (5)$$
$$L_s \frac{di_q}{dt} = -\omega L_s i_d - R_s i_q + g_q - v_q. \quad (6)$$

Here, L_s and R_s are the inductance and the resistance of the output filter inductor. Combining (4)-(6) and using the notation

$$R = nR_s, \quad L = nL_s,$$

we get the differential equations of the grid currents:

$$L\frac{di_d}{dt} = -Ri_d + \omega L i_q + V\sin\delta + (n-1)\eta_d, \quad (7)$$
$$L\frac{di_q}{dt} = -\omega L i_d - Ri_q - m i_f \omega + V\cos\delta + (n-1)\eta_q. \quad (8)$$

The angular frequency satisfies the *swing equation*

$$J\frac{d\omega}{dt} = T_m - T_e - D_p\omega + D_p\omega_n, \quad (9)$$

where $J > 0$ is the *virtual inertia* of the rotor, $T_m > 0$ is the *nominal active mechanical torque* from the prime mover,

$$T_e = -m i_f (i_q + \xi_q) \quad (10)$$

is the estimated *electric torque* computed using the measured output currents and $D_p > 0$ is the *frequency droop constant*. The torque T_m is computed from P_{set} (the desired active

power) and Q_{set} (the desired reactive power) using the formula

$$T_m\omega_n = P_{set} + R\frac{P_{set}^2 + Q_{set}^2}{V^2}. \tag{11}$$

The justification for this formula will be in Proposition 3. From the definition of the power angle δ:

$$\frac{d\delta}{dt} = \omega - \omega_g. \tag{12}$$

The instantaneous inverter output reactive power is

$$Q = v_q i_d - v_d i_q = V[i_q \sin\delta - i_d \cos\delta], \tag{13}$$

see for instance [20, eq.(16)]. Due to the measurement errors, the following estimate Q_{est} of Q is computed in the basic synchronverter control algorithm: at equilibrium

$$\begin{aligned} Q_{est} &= (v_q + \eta_q)(i_d + \xi_d) - (v_d + \eta_d)(i_q + \xi_q) \\ &\approx V[(i_q + \xi_q)\sin\delta - (i_d + \xi_d)\cos\delta] + \eta_q i_d - \eta_d i_q, \end{aligned} \tag{14}$$

where we have neglected products of error terms.

The field current i_f evolves according to [20, eq.(15)], which represents the integral controller that adjusts the field current:

$$M_f\frac{di_f}{dt} = \frac{1}{K}\left[\tilde{Q} - Q_{est}\right], \tag{15}$$

$$\tilde{Q} = Q_{set} + D_q\left(v_{set} - \sqrt{\frac{2}{3}}V\right). \tag{16}$$

In (15), $K > 0$ is a large constant. The value $\tilde{Q}$ represents a compromise between tracking the reference reactive power Q_{set} and tracking the reference value v_{set} for the amplitude of v. Tracking v_{set} makes sense only if the inverter is connected to the infinite bus through a line impedance, and not directly, as in our model. Still, our model reflects the full field current controller. In (16), $D_q > 0$ is the *voltage droop coefficient* and V is as in (1). Denote

$$k = \sqrt{\frac{3}{2}}\frac{V}{K}.$$

The fifth order grid-connected synchronverter model that includes voltage and current measurement errors can be constructed by combining the equations (7)-(15), with state vector $\mathbf{z} \in \mathbb{R}^5$. The input of this model is the measurement error vector $\mathbf{u} \in \mathbb{R}^4$. The components of $\mathbf{z}$ and $\mathbf{u}$ are

$$\mathbf{z} = \begin{bmatrix} i_d \\ i_q \\ \omega \\ \delta \\ i_f \end{bmatrix}, \quad \mathbf{u} = \begin{bmatrix} \eta_d \\ \eta_q \\ \xi_d \\ \xi_q \end{bmatrix}. \tag{17}$$

We write this model as a nonlinear dynamical system:

$$\mathbf{H}\dot{\mathbf{z}} = \mathbf{A}(\mathbf{z})\mathbf{z} + \mathbf{B}(\mathbf{z})\mathbf{u} + f(\mathbf{z}), \tag{18}$$

where

$$\mathbf{H} = \begin{bmatrix} L & 0 & 0 & 0 & 0 \\ 0 & L & 0 & 0 & 0 \\ 0 & 0 & J & 0 & 0 \\ 0 & 0 & 0 & 1 & 0 \\ 0 & 0 & 0 & 0 & m \end{bmatrix}, \quad f(\mathbf{z}) = \begin{bmatrix} V\sin\delta \\ V\cos\delta \\ T_m + D_p\omega_n \\ -\omega_g \\ \frac{k}{V}\tilde{Q} \end{bmatrix},$$

$$\mathbf{A}(\mathbf{z}) = \begin{bmatrix} -R & \omega L & 0 & 0 & 0 \\ -\omega L & -R & -mi_f & 0 & 0 \\ 0 & mi_f & -D_p & 0 & 0 \\ 0 & 0 & 1 & 0 & 0 \\ k\cos\delta & -k\sin\delta & 0 & 0 & 0 \end{bmatrix},$$

and

$$\mathbf{B}(\mathbf{z}) = \begin{bmatrix} n-1 & 0 & 0 & 0 \\ 0 & n-1 & 0 & 0 \\ 0 & 0 & 0 & mi_f \\ 0 & 0 & 0 & 0 \\ \frac{k}{V}i_q & -\frac{k}{V}i_d & k\cos\delta & -k\sin\delta \end{bmatrix}.$$

Remark 1: The model in [16], [20] uses a "saturating integrator" for integrating the right-hand side of (15), in order to ensure that i_f stays in a reasonable operating range. This helps in proving stability with a relatively large region of attraction in [16], and it helps the system overcome faults. In the analysis of this paper, we ignore the saturating integrator, our model uses just a simple integrator, which is reasonable since in practice, the saturation limits are very rarely reached, it happens only during faults.

Remark 2: The instantaneous active power P from the synchronverter to the grid (see also [20, eq.(17)]) is

$$P = v_d i_d + v_q i_q = -V[i_d \sin\delta + i_q \cos\delta]. \tag{19}$$

Solving the equations (13) and (19) for the dq currents, we get the following nice formula:

$$\begin{bmatrix} i_q \\ i_d \end{bmatrix} = -\frac{1}{V}\begin{bmatrix} \cos\delta & -\sin\delta \\ \sin\delta & \cos\delta \end{bmatrix}\begin{bmatrix} P \\ Q \end{bmatrix}. \tag{20}$$

III. EQUILIBRIUM POINTS OF THE FIFTH ORDER GRID-CONNECTED SYNCHRONVERTER

In this section we briefly recall some results on the equilibrium points of the fifth order model (18) (of a grid-connected synchronverter), based on [16]. In the sequel, angles are always regarded modulo 2π, i.e., δ and $\delta + 2\pi$ are considered to be the same angle.

To find the equilibrium points of the model (18), we set $\mathbf{u} = 0$ and $\dot{\mathbf{z}} = 0$ in (18). The following result, taken from [16, Sect. 4], concerns mainly the equation that must be satisfied by the active power P at an equilibrium point.

Proposition 3: Consider the model (18), with $\mathbf{u} = 0$. We assume that $R, L, J, m, D_p, D_q, V, \omega_g, \omega_n, v_{set} > 0$ and the real parameters T_m and Q_{set} are given. We denote

$$\tilde{T}_m = T_m + D_p(\omega_n - \omega_g),$$

and we use the notation $\tilde{Q}$ introduced in (16). A necessary condition for this system to have equilibrium points is

$$4R^2\tilde{Q}^2 \le V^4 + 4RV^2\tilde{T}_m\omega_g. \tag{21}$$

At every equilibrium point of this system we have

$$\omega^e = \omega_g, \quad T_e = \tilde{T}_m, \quad Q = \tilde{Q}, \tag{22}$$

and P satisfies the equation

$$\tilde{T}_m \omega_g = P + R\frac{P^2 + \tilde{Q}^2}{V^2}. \tag{23}$$

Remark 4: The formula (23) is used in the synchronverter algorithm to determine the value of the parameter T_m, if the reference values P_{set} and Q_{set} are given and if some estimate (for instance, zero) is adopted for the differences $\omega_n - \omega_g$ and $v_{set} - \sqrt{2/3}V$. If we adopt the estimates $\omega_g = \omega_n$ and $\sqrt{2/3}V = v_{set}$, then this computation of T_m reduces to (11).

Remark 5: The equilibrium points of (18), with $\mathbf{u} = 0$, come in symmetric pairs. Indeed, if $\mathbf{z}^e = [i_d^e \; i_q^e \; \omega_g \; \delta^e \; i_f^e]^\top$ is such an equilibrium point, then also

$$\tilde{\mathbf{z}}^e = [-i_d^e \; -i_q^e \; \omega_g \; \delta^e + \pi \; -i_f^e]^\top$$

is an equilibrium point. The intuition behind this is clear: if we rotate the rotor by a half circle and at the same time invert the current i_f in the rotor, then due to the symmetry of the rotor we get the same rotor field (in the fixed coordinate system of the stator). Thus, if the system was at equilibrium before this rotation by π, then it must be again at equilibrium.

Remark 6: There is an exceptional infinite set of equilibrium points of the system (18), which corresponds to the parameters T_m and Q_{set} chosen such that

$$\tilde{T}_m = 0, \quad \tilde{Q} = -\frac{V^2 \omega_g L}{R^2 + \omega_g^2 L^2} =: Q_M. \tag{24}$$

In these equilibria, $i_f^e = 0$, so that the rotor is inactive, the angle δ^e can be chosen freely, and the currents i_d and i_q can then be computed from (20). The active power in these equilibrium points is

$$P_M = -\frac{V^2 R}{R^2 + \omega_g^2 L^2}. \tag{25}$$

Denote $M = (P_M, Q_M) \in \mathbb{R}^2$. The set of equilibrium points of (18) where $i_f^e > 0$ can be parametrized by the corresponding powers (P, Q), and then it is a two-dimensional manifold diffeomorphic to $\mathbb{R}^2 \setminus \{M\}$.

Remark 7: The real system can never reach an equilibrium point with the property $i_f^e \leq 0$. The reason is that the synchronverter algorithm that controls the true system has a saturating integrator to compute i_f, as explained in Remark 1, and the minimum value of i_f is set to be positive.

The following theorem, also taken from [16, Sect. 4], tells us how to compute the equilibrium points of (18) corresponding to given values of the parameters $\tilde{T}_m$ and $\tilde{Q}$, except for the exceptional values discussed in Remark 6.

Theorem 8: We work under the assumptions of Proposition 3, with $\tilde{T}_m$ and $\tilde{Q}$ given. Then the model (18), with $\mathbf{u} = 0$, has equilibrium points if and only if (21) holds.

Suppose that (21) is true, and let us denote by P_l and P_r the two real solutions of (23), so that $P_l \leq P_r$, and $\frac{P_l + P_r}{2} = -\frac{V^2}{2R}$. At every equilibrium point $\mathbf{z}^e = [i_d^e \; i_q^e \; \omega_g \; \delta^e \; i_f^e]^\top$ that corresponds to the given $\tilde{T}_m$ and $\tilde{Q}$, we have $P = P_l$ or $P = P_r$.

Let P be the active power at an equilibrium point $\mathbf{z}^e$ as above. Assume that P and $\tilde{Q}$ are not the exceptional pair M described in (24) and (25). Then the equilibrium angle δ^e satisfies

$$\tan \delta^e = \frac{\omega_g L P - R\tilde{Q}}{RP + \omega_g L \tilde{Q} + V^2}. \tag{26}$$

If the angle δ^e is measured modulo 2π, and (21) holds with strict inequality, then the model (18) has precisely four equilibrium points. Two of them, denoted by $\mathbf{z}_l^e$ and $\mathbf{z}_r^e$, have the property that $i_f^e > 0$. At $\mathbf{z}_l^e$, $P = P_l$, and at $\mathbf{z}_r^e$, $P = P_r$. There are also the two symmetric equilibrium points $\tilde{\mathbf{z}}_l^e$ and $\tilde{\mathbf{z}}_r^e$ where $i_f^e < 0$, as described in Remark 5.

If (21) holds with equality, then $P_l = P_r = -V^2/2R$ and the model has precisely two equilibrium points, which are a symmetric pair, as described in Remark 5.

Once δ^e has been found, the values i_d^e and i_q^e can be computed from (20), and i_f can be computed from (10) (with $\xi_q = 0$ and $T_e = \tilde{T}_m$).

IV. SMALL SIGNAL ANALYSIS

We consider the output of the system (18) to be the grid currents (in dq coordinates), $\mathbf{y} = [i_d \; i_q]^\top$. We linearize this system near the stable equilibrium point, to explore the small signal behavior of the dq currents as a result of the measurement errors. Define the small signal state variables

$$\hat{i}_d = i_d - i_d^e, \quad \hat{i}_q = i_q - i_q^e, \quad \hat{\omega} = \omega - \omega_g,$$
$$\hat{\delta} = \delta - \delta^e, \quad \hat{i}_f = i_f - i_f^e.$$

Denote $\hat{\mathbf{z}} = [\hat{i}_d \; \hat{i}_q \; \hat{\omega} \; \hat{\delta} \; \hat{i}_f]^\top$ (the state deviation from equilibrium) and $\hat{\mathbf{y}} = [\hat{i}_d \; \hat{i}_q]^\top$ (the output deviation).

We define a function $F : \mathbb{R}^5 \times \mathbb{R}^4 \to \mathbb{R}^5$ as follows:

$$F(\mathbf{z}, \mathbf{u}) = \mathbf{A}(\mathbf{z})\mathbf{z} + \mathbf{B}(\mathbf{z})\mathbf{u} + f(\mathbf{z}). \tag{27}$$

The linearized system will be of the form

$$\mathbf{H}\dot{\hat{\mathbf{z}}} = \mathbf{A}_{lin}\hat{\mathbf{z}} + \mathbf{B}_{lin}\mathbf{u}, \quad \hat{\mathbf{y}} = \mathbf{C}_{lin}\hat{\mathbf{z}}, \tag{28}$$

where $\mathbf{A}_{lin}$ is the Jacobian $\mathbf{A}_{lin} = \partial F/\partial \mathbf{z}$ computed at the equilibrium point $\mathbf{z}^e$ with $\mathbf{u} = 0$, while $\mathbf{B}_{lin} = \partial F/\partial \mathbf{u}$ (evaluated at the same point). The matrix $\mathbf{C}_{lin}$ is simply the projector from $\mathbb{R}^5$ to $\mathbb{R}^2$ by selecting the first two components. Denote again $k = \sqrt{\frac{3}{2}}\frac{V}{K}$, then the matrices of the linearized model (28) are

$$\mathbf{A}_{lin} = \begin{bmatrix} -R & \omega_g L & Li_q^e & V\cos\delta^e & 0 \\ -\omega_g L & -R & -mi_f^e - Li_d^e & -V\sin\delta^e & -m\omega_g \\ 0 & mi_f^e & -D_p & 0 & mi_q^e \\ 0 & 0 & 1 & 0 & 0 \\ k\cos\delta^e & -k\sin\delta^e & 0 & -v_0 & 0 \end{bmatrix},$$

where

$$v_0 = k\left(i_d^e \sin\delta^e + i_q^e \cos\delta^e\right),$$

$$\mathbf{B}_{lin} = \begin{bmatrix} n-1 & 0 & 0 & 0 \\ 0 & n-1 & 0 & 0 \\ 0 & 0 & 0 & mi_f^e \\ 0 & 0 & 0 & 0 \\ \frac{k}{V}i_q^e & -\frac{k}{V}i_d^e & k\cos\delta^e & -k\sin\delta^e \end{bmatrix},$$

and

$$\mathbf{C}_{lin} = \begin{bmatrix} 1 & 0 & 0 & 0 & 0 \\ 0 & 1 & 0 & 0 & 0 \end{bmatrix}.$$

The transfer function $\mathbf{G}(s) = \mathbf{C}_{lin}[sI - \mathbf{H}^{-1}\mathbf{A}_{lin}]^{-1}\mathbf{H}^{-1}\mathbf{B}_{lin}$ can be computed from the above matrices, but its analytic expression is very complicated.

Naturally, we are only interested in asymptotically stable equilibrium points, i.e., those where $\mathbf{H}^{-1}\mathbf{A}_{lin}$ is a stable matrix. There is a detailed discussion on stable equilibrium points of (18) in our paper [16], and we sketch a result from there. We assume that $R, L, J, m, D_p, D_q, V, \omega_g, \omega_n, v_{set} > 0$ are fixed (as in Proposition 3). The real parameters T_m and Q_{set} can be changed by the user, giving rise to a manifold of equilibrium points. We consider only the submanifold where $i_f > 0$ (there is also a symmetric submanifold with $i_f < 0$, as explained in Remark 5). This submanifold (with $i_f > 0$) can be parametrized by the powers P and Q: for every pair $(P, Q) \in \mathbb{R}^2$ except for the singular point M defined in (24) and (25), there is a single equilibrium point with $i_f > 0$.

We define a point $C \in \mathbb{R}^2$ by $C = (-V^2/2R, 0)$. We denote by $\mathcal{S}$ the angular sector in $\mathbb{R}^2$ that is bounded by the line CM and the vertical line passing through C, see Figure 4, which has been adapted from [16]. Normally, the state of a synchronverter is kept in a region contained in $\mathcal{S}$, because for well chosen parameters, equilibrium points for which $(P, Q) \in \mathcal{S}$ and $P^2 + Q^2$ is not too large, are stable. Below we try to explain this stability issue a bit more, but for the full details we refer to [16].

It has been shown in [16, Sect. 5] that if (P, Q) is in $\mathcal{S}$ and a certain 4th order model is stable (which is often the case), and if (P, Q) is not too large (which is true within the normal operating range of the inverter), then for $k > 0$ sufficiently small, the model (18) is asymptotically stable around the corresponding equilibrium point. This fact is illustrated in Figure 4, which refers to Example 1 later in this section. The figure shows the points C and M for this example, the sector $\mathcal{S}$ and the part of the sector where the stability of the fourth order model is true, highlighted in green. This being a converter of nominal power 9 kW, the region of interest $\mathcal{H}$ is, say the disk defined by $\sqrt{P^2 + Q^2} \leq 20$ kW, shown in Figure 4. Within $\mathcal{H}$, we see that the green part is exactly $\mathcal{H} \cap \mathcal{S}$. The figure also shows the set of stable equilibrium points of the model for four different values of k.

In the following, we will illustrate the excessive sensitivity of the synchronverter to measurement errors by using Bode amplitude plots for a numerical example.

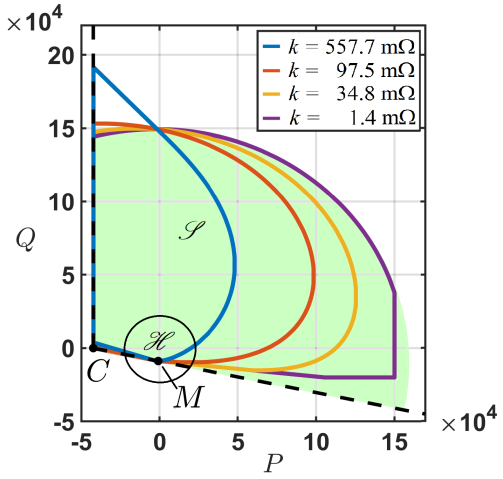

FIGURE 4. The stable regions of the grid-connected synchronverter from Example 1, for four values of the gain k. Only the region $\mathcal{H}$ (a disk with center at the origin) is of practical interest, and within the disk $\mathcal{H}$, stability holds for points (P, Q) above the line CM.

Example 1: We use the parameters of a synchronverter designed to supply a nominal active power of 9 kW to a grid with frequency $\omega_g = 100\pi$ rad/sec (50 Hz) and line voltage $V = 230\sqrt{3}$ Volts. This is based on a real inverter that we have built, see [15]. The parameters are: $J = 0.2$ kg·m^2/rad, $D_p = 3$ N·m/(rad/sec), $L_s = 2.27$ mH, $R_s = 0.075\ \Omega$, $K = 5000$ A, $n = 25$, $D_q = 0$ VAr/Volt, $m = 3.5$ H. We take $T_m = 31.69$ Nm (according to [20, eq.(24)], this mechanical torque corresponds to $P_{set} = 9000$ W and $Q_{set} = 0$ VAr). For simplicity we let $v_{set} = \sqrt{\frac{2}{3}}V = 325.26$ Volt, $Q_{set} = 0$ VAr, so that $\tilde{Q} = 0$, and $m = 1$. We have $R = nR_s = 1.875\ \Omega$, $L = nL_s = 56.75$ mH, $\phi = 83.99°$, and $I_f = [1.3; 13.4]$. Note that at the grid frequency, positive (negative) measurement error sequences are mapped through the Park transformation into constants (sinusoids with frequency $2\omega_g$). Therefore, when looking at the Bode plots from Figures 5 and 6, we have to focus our attention to the frequency range $[0, 2\omega_g]$.

From Theorem 8 we know that there are four equilibrium points. We are interested in the two that have $i_f^e > 0$:

$$\begin{bmatrix} i_{d,1}^e \\ i_{q,1}^e \\ \omega_g \\ \delta_1^e \\ i_{f,1}^e \end{bmatrix} = \begin{bmatrix} -15.24 \\ -16.68 \\ 314.16 \\ 42.42° \\ 0.54 \end{bmatrix}, \quad \begin{bmatrix} i_{d,2}^e \\ i_{q,2}^e \\ \omega_g \\ \delta_2^e \\ i_{f,2}^e \end{bmatrix} = \begin{bmatrix} -235.04 \\ -2.38 \\ 314.16 \\ -90.58° \\ 3.81 \end{bmatrix}.$$

Some routine computations show that the first equilibrium point is stable and the second one is unstable.

We mention that if we compute the active power P at the above two equilibrium points according to (19), we get that $P = 9$ kW at the stable equilibrium point (which is exactly P_{set}) while $P = -93.64$ kW at the unstable equilibrium point. This corresponds to what we expect based on Theorem 8. It can be verified that the two symmetric equilibrium points $\tilde{\mathbf{x}}_1^e$ and $\tilde{\mathbf{x}}_2^e$ (where $i_f^e < 0$) are unstable.

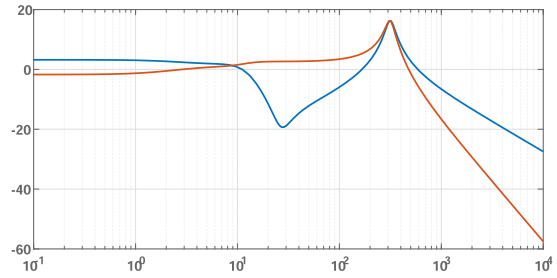

(a) From η_d to i_d (blue) and from η_q to i_d (red)

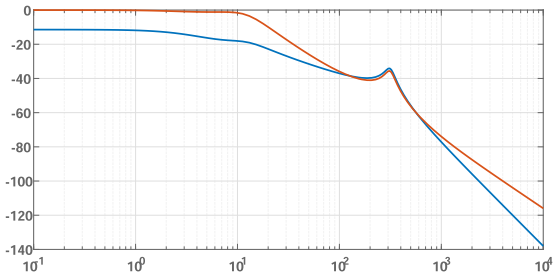

(b) From ξ_d to i_d (blue) and from ξ_q to i_d (red)

FIGURE 5. The gains from the measurement errors to i_d, near the stable equilibrium point for Example 1. These are Bode amplitude plots, with the axes in dB and in Hz.

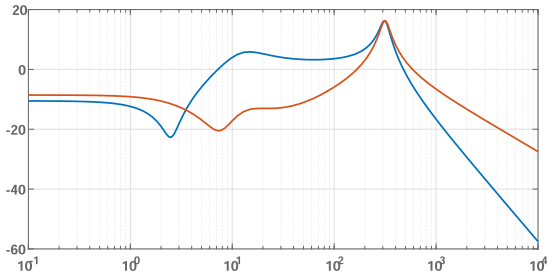

(a) From η_d to i_q (blue) and from η_q to i_q (red)

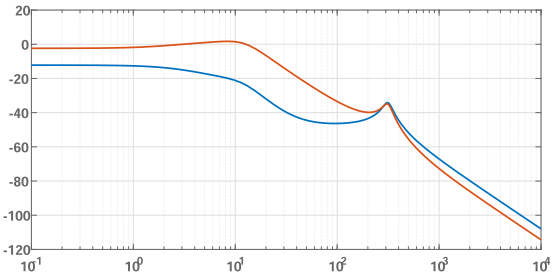

(b) From ξ_d to i_q (blue) and from ξ_q to i_q (red)

FIGURE 6. The gains from the measurement errors to i_q, near the stable equilibrium point for Example 1. These are Bode amplitude plots, with the axes in dB and in Hz.

It is *not true* that one of the two equilibrium points with $i_f > 0$ (whose existence is guaranteed by Theorem 8) has to be stable. Indeed, if we modify this example by taking $K = 100$ A (instead of 5000 A), then both equilibrium points with $i_f > 0$ are unstable. It is possible that, similarly to the main result of [21], under additional assumptions on the parameters, (18) has a stable equilibrium point that is almost globally asymptotically stable - this is an open question.

Figure 5 shows the Bode amplitude plots of the small signal transfer functions from each measurement error to i_d, at the stable equilibrium point. Figure 5(a) shows a large gain from η_d to i_d at the grid frequency (which corresponds to the frequency zero in dq coordinates). This gain is of the order of 3 dB, which means that a voltage measurement error of 4 V (entirely plausible, as it is about the resolution of the voltage sensor) would cause a current deviation of about 6 A, which is unacceptable. (This particular conclusion was already presented in Section I, based on an intuitive argument, while here we have deduced it from more precise computations.) An even larger peak of the gain from η_d to i_d occurs around the frequency 30 Hz in dq coordinates. The gain from η_q to i_d is almost as large as the gain from η_d to i_d, and again we see a peak around 30 Hz.

Figure 6 shows the Bode amplitude plots of the transfer functions from the measurement errors to i_q. The plots in Figure 6 are less critical than those in Figure 5. Note that in both Figures 5 and 6, the gains from the current measurement errors to the output currents are less disturbing than the gains from the voltage measurement errors to the output currents.

V. SENSITIVITIES OF THE SYNCHRONVERTER WITH IDEAL CURRENT SOURCES AT ITS OUTPUTS

In the previous section, we have shown that the output currents of a classical synchronverters are very sensitive to the grid voltage measurement errors. To overcome this problem, we propose to use controlled current sources at the output of the converter. We will modify the basic control algorithm accordingly. Similar modifications have been proposed, for instance, in [3], [10], [17], [19], [22], [26]. An interesting recent synchronverter design is in [7], which proposes to include an output admittance synthesizer in the control algorithm of the inverter, that enables to allocate desired output admittance values at multiples of the grid frequency, separately for the positive and negative sequence components, and without the need to measure the grid voltages. This technique allows to obtain very clean sinusoidal output currents (it is an interesting question whether this is desirable for the grid). Our design will behave like a SG, so that if the grid voltages are distorted or unbalanced, then the currents will also be distorted or unbalanced, since they are "trying to counteract" the distortions on the grid.

A simplified representation of the proposed modified AC output power circuit of the converter is as shown on Figure 7, that shows only one out of three identical phases. In this modified version of the synchronverter algorithm, we use the virtual currents $i_{virt} = [i_{virt,a}\ i_{virt,b}\ i_{virt,c}]^\top$ as references for the current sources and also for computing the electric torque. The virtual impedance consists of an inductor $L_g \approx nL_s$ in series with a resistor $R_g \approx nR_s$. Since L_g and R_g are much larger than L_s and R_s, the voltage measurement errors will influence the output currents much less, as we show below.

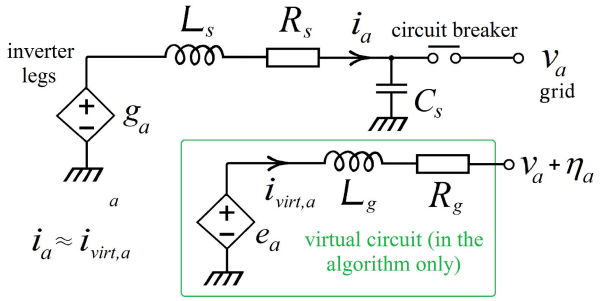

FIGURE 7. A modified synchronverter with controlled current sources at its output (only one phase is shown). e_a is the synchronous internal voltage.

We denote again by $\eta = [\eta_a\ \eta_b\ \eta_c]^\top$ the voltage measurements errors in the three phases. Then the virtual current in phase a satisfies the differential equation

$$L_g \frac{d\, i_{virt,a}}{d\, t} + R_g i_{virt,a} = e_a - (v_a + \eta_a)$$

and we have similar equations for the other phases.

Applying the Park transformation and using (4), (3), we get

$$L_g \frac{d\, i_{virt,d}}{d\, t} = -R_g i_{virt,d} + \omega L_g i_{virt,q} + V \sin\delta - \eta_d, \quad (29)$$

$$L_g \frac{d\, i_{virt,q}}{d\, t} = -\omega L_g i_{virt,d} - R_g i_{virt,q} - m i_f \omega + V \cos\delta - \eta_q. \quad (30)$$

The measured synchronverter output currents (in dq coordinates) are $(i_{virt,d} + \tilde{\xi}_d)$, $(i_{virt,q} + \tilde{\xi}_q)$, where the measurement errors $\tilde{\xi}_d, \tilde{\xi}_q$ are partly due to the original measurement errors ξ_d, ξ_q and partly due to the imperfection of the controlled current sources.

The electric torque computed using i_{virt} is

$$T_e = -m i_f i_{virt,q}$$

and the estimate Q_{est} of the instantaneous output power is computed in the control algorithm by

$$\begin{aligned} Q_{est} &= (v_q + \eta_q) i_{virt,d} - (v_d + \eta_d) i_{virt,q} \\ &\approx V[i_{virt,q} \sin\delta - i_{virt,d} \cos\delta] + \eta_q i_{virt,d} - \eta_d i_{virt,q}. \end{aligned} \quad (31)$$

In the model of the new system, the currents i_d, i_q are replaced with $i_{virt,d}, i_{virt,q}$. Comparing the equations (29), (30) with their counterparts from (7), (8) (remembering that $L_g \approx nL_s = L$, $R_g \approx nR_s = R$) shows that what has changed is that the influence of η_d, η_q on the (virtual) currents has been decreased by a factor $1/(n-1)$. The equilibrium points of the new system are the same as for the model (18). In the linearization of the new system, that looks similarly to (28), the matrices $\mathbf{A}_{lin}$ and $\mathbf{C}_{lin}$ remain the same, but in the matrix $\mathbf{B}_{lin}$ the terms $n-1$ have been replaced by 1. The other rows of $\mathbf{B}_{lin}$ remain unchanged, so that we do not get an overall $(n-1)$ times reduction of the influence of η_d, η_q, but we still get a substantial improvement, as we shall see in the Bode plots corresponding to Example 1 from the previous section.

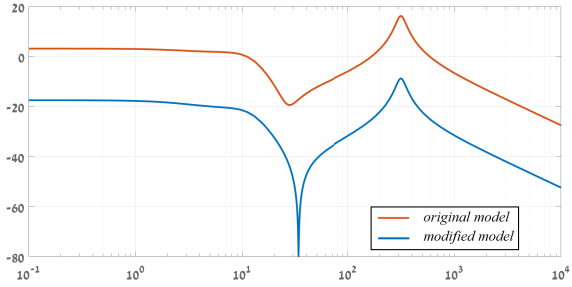

(a) From η_d to i_d

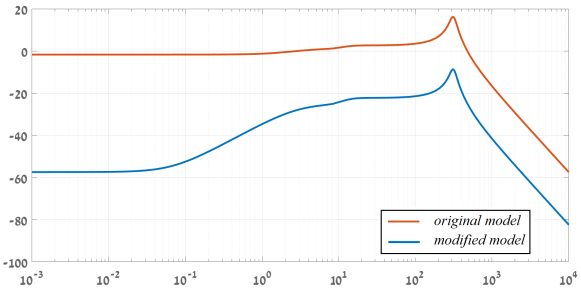

(b) From η_q to i_d

FIGURE 8. The gains from the measurement errors to i_d, near the stable equilibrium for Example 1, for the original and the modified system. These are Bode amplitude plots, with the axes in dB and in Hz.

Figure 8 shows a comparison between the Bode amplitude plots of the small signal transfer functions from each measurement error to i_d, at the stable equilibrium point for the original and modified system. Figure 8(a) shows a decrease of approximately 20 dB for the gain from η_d to i_d at the grid frequency (which corresponds to the frequency zero in dq coordinates). This new gain is of the order of -17 dB, which means that a voltage measurement error of 4 V (the resolution of the voltage sensor) would cause a current deviation of about 0.56 A, which is acceptable.

Figure 9 shows the Bode amplitude plots of the transfer functions from the measurement errors to i_q for the original and the modified system. These plots also show a considerable improvement due to the use of the current sources.

VI. EXPERIMENTAL RESULTS

We have built a small 3 level inverter with nominal power 2.5kW designed for grid voltages up to 230V rms, see Figure 10. The output filter parameters are $L_s = 7.2$ mH, $R_s = 0.2\Omega$, with filter capacitor $C_s = 2.2\mu$F, with an ST microcontroller executing the algorithm every 100μsec. We have realized on this inverter both the "old" algorithm from [20] with $J = 0.04kg \cdot m^2$, $D_p = 0.06kg \cdot m^2/s$, $D_q = 0$, $K = 2000$ A and $n = 20$, as well as the algorithm with current sources described here, that we call the "new" algorithm for brevity. The details of the current source design are not essential for this paper and would take much space, so we give them separately in [14]. For the new algorithm we have chosen $L_g = nL_s$ and $R_g = nR_s$, and the other parameters are the same as for the old algorithm, so that if there would be no measurement errors, then in both cases the grid connected

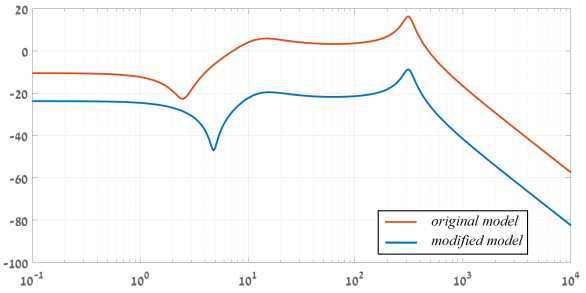

(a) From η_d to i_q

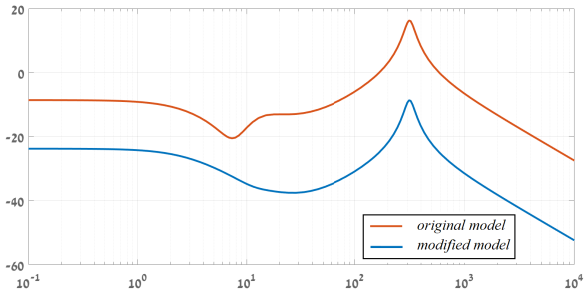

(b) From η_q to i_q

FIGURE 9. The gains from the measurement errors to i_q, near the stable equilibrium for Example 1, for the original and the modified system. These are Bode amplitude plots, with the axes in dB and in Hz.

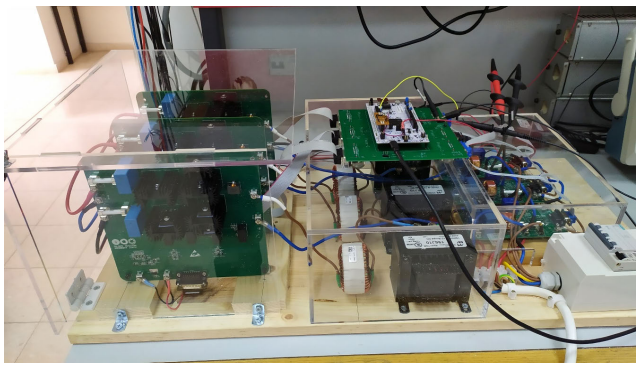

FIGURE 10. The inverter used in our experiments.

inverter would follow the model (18) with $u = 0$. This allows us to make a realistic comparison of the sensitivity of the currents to measurement errors using the two algorithms.

In both algorithms, there are various extra details that we do not describe here: start-up procedures, current limitations, torque limitations, various low-pass filters to reduce the noise, as well as large virtual capacitors in series with the output, to prevent DC currents. These extra details have very little influence when the inverter is working normally.

Because of the high sensitivity of the old algorithm to measurement errors, we have cautiously done all these comparison experiments at a low grid voltage of 70 V rms (using an autotransformer). Figure 11 shows the grid voltages measured at the inverter legs at idle. It is clear that these voltages are distorted, and moreover the three phases are not balanced, with phase a having 1.3% lower voltage than phase c and phase b having 2.7% lower voltage than phase c.

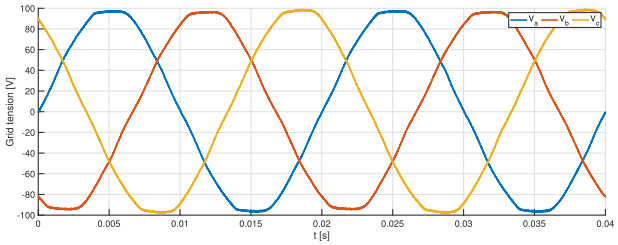

FIGURE 11. The grid voltages measured at the inverter output with the inverter disconnected.

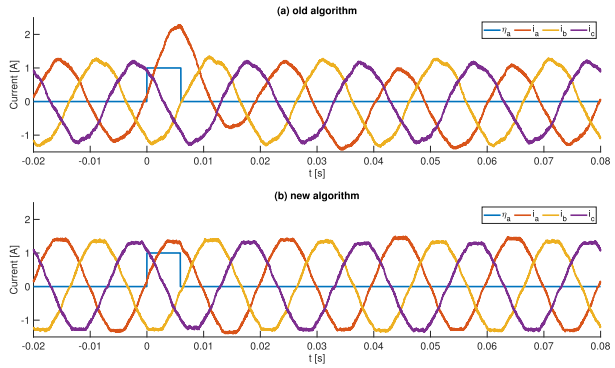

FIGURE 12. Grid currents when the inverter works at steady state and a rectangular pulse shaped measurement error is introduced at time $t = 0$. (a) With the old algorithm. (b) With the new algorithm. The blue curve, denoted η_a, indicates a 5 msec measurement error of 4V added to phase a.

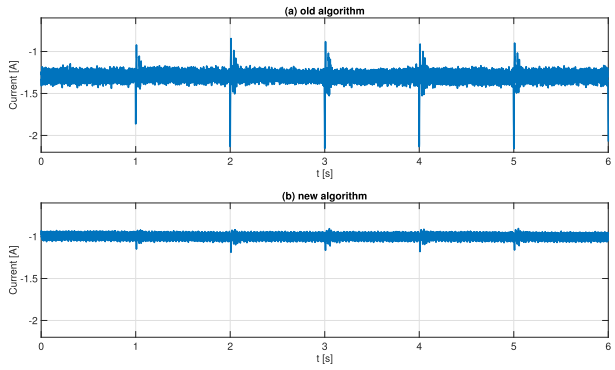

FIGURE 13. The grid current i_d during repeated 5 msec measurement error pulses of 4V on phase a.

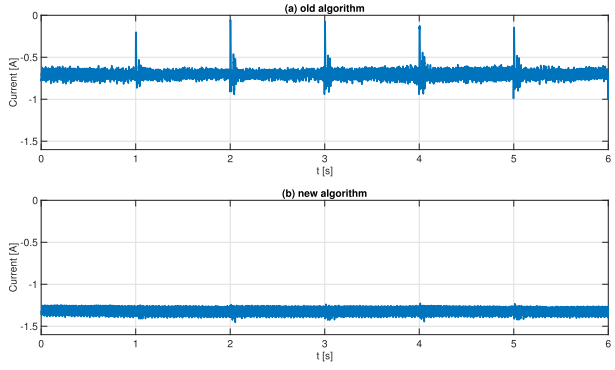

FIGURE 14. The grid current i_q during repeated 5 msec measurement error pulses of 4V on phase a.

Figure 12 shows the grid currents of the inverter running at steady state, with $P_{set} = 200$ W and $Q_{set} = 40$ VAr,

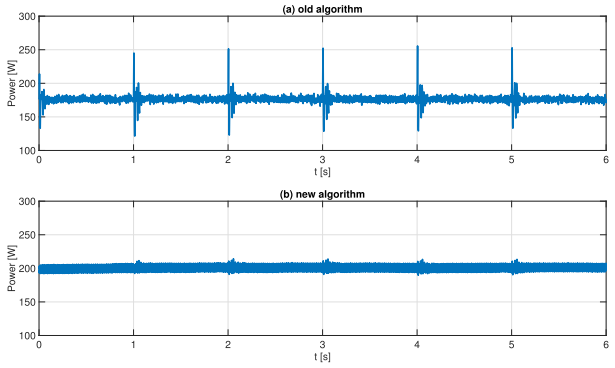

FIGURE 15. The active power during repeated 5 msec measurement error pulses of 4V on phase a.

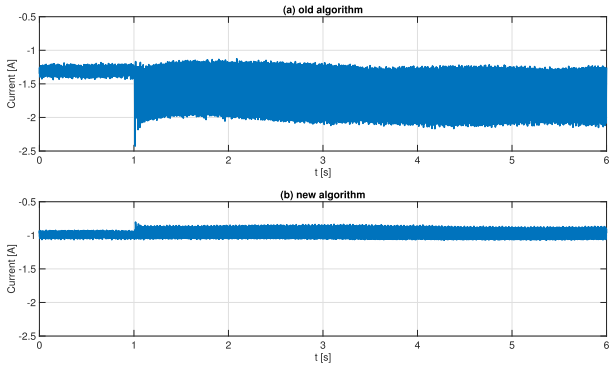

FIGURE 16. The current i_d when a 5% calibration error is introduced on phase a at $t = 1$.

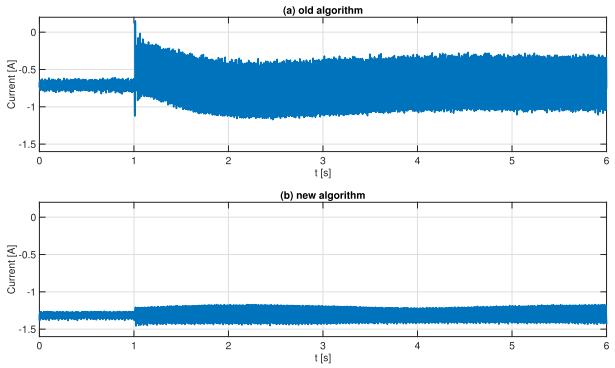

FIGURE 17. The current i_q when a 5% calibration error is introduced on phase a at $t = 1$.

as measured by external Hall sensors not connected to the inverter. The currents are distorted because the grid voltage is distorted, as we have seen earlier. At a moment denoted $t = 0$, we artificially introduce a voltage measurement error of 4V lasting for 5 msec in phase a, via the inverter control software. With the old algorithm, this measurement error causes a considerable overshoot of the current in phase a, lasting for about one period. The same experiment conducted with the new algorithm shows no visible impact on the currents.

Figures 13 and 14 show the influence of measurement error pulses on phase a (of the same amplitude and duration as before) on i_d and i_q. The pulses are repeated every second. The data shown has been extracted from the microcontroller. We see that the impact of the pulses is significantly larger with the old algorithm than with the new one.

Figure 15 shows the impact of these pulses on the active power. In the case of the old algorithm the calculated active power exhibits disturbances lasting for about 100 msec.

We have conducted experiments where at first we have let the inverter work at steady state, and then at $t = 1$ we have artificially introduced a calibration error of 5% on phase a, proportional to the measured signal. Figures 16 and 17 show the currents i_d and i_q, as extracted from the microcontroller. This calibration error introduces disturbances with an amplitude of about 380 mA in i_d and i_q with the old algorithm, while only about 120 mA with the new algorithm.

VII. CONCLUSION

We have presented the sensitivity analysis for a fifth order synchronverter model connected to an infinite bus, with respect to voltage and current measurement errors. We have shown that the sensitivity of the grid currents to voltage measurement errors is too large to be acceptable, leading to distorted grid currents (as observed in experiments). We have proposed a modification of the basic control algorithm by using current sources controlled by virtual currents generated in the algorithm, via virtual output impedances. Computing the sensitivities for an example, we have seen that this modification dramatically improves the synchronverter sensitivities. The design of these current sources, integrated with the synchronverter design, is a long story that will be discussed in the paper [14]. Our computations and simulation results are well supported by experimental results, where we have compared the sensitivity of the currents of an inverter running according to the algorithm from [20] against the new algorithm proposed here. To make the comparison fair, we have taken the virtual impedances in the new algorithm equal to n times the real filter impedance of the inverter, so that the mathematical models describing the two inverters are equal, except for the influence of the measurement errors.

ACKNOWLEDGMENT

The authors are grateful for the help from the SGI-Lab at the Joint Research Center of the European Commission, Ispra, Italy.

REFERENCES

[1] J. Alipoor, Y. Miura, and T. Ise, "Distributed generation grid integration using virtual synchronous generator with adoptive virtual inertia," in *Proc. IEEE Energy Convers. Congr. Expo. (ECCE)*, Denver, CO, USA, Sep. 2013, pp. 4546–4552.

[2] R. Aouini, B. Marinescu, K. B. Kilani, and M. Elleuch, "Synchronverter-based emulation and control of HVDC transmission," *IEEE Trans. Power Syst.*, vol. 31, no. 1, pp. 278–286, Jan. 2016.

[3] M. Ashabani and J. Jung, "Synchronous voltage controllers: Voltage-based emulation of synchronous machines for the integration of renewable energy sources," *IEEE Access*, vol. 8, pp. 49497–49508, 2020.

[4] N. Barabanov, J. Schiffer, R. Ortega, and D. Efimov, "Conditions for almost global attractivity of a synchronous generator connected to an infinite bus," *IEEE Trans. Autom. Control*, vol. 62, no. 10, pp. 4905–4916, Oct. 2017.

[5] H.-P. Beck and R. Hesse, "Virtual synchronous machine," in *Proc. 9th Int. Conf. Electr. Power Quality Utilisation (EPQU)*, Barcelona, Spain, Oct. 2007, pp. 1–6.

[6] M. Blau and G. Weiss, "Synchronverters used for damping inter-area oscillations in two-area power systems," in *Proc. Int. Conf. Renew. Energies Power Quality (ICREPQ)*, Salamanca, Spain, Mar. 2018, pp. 1–6.

[7] C. A. Busada, S. Gomezjorge, and J. A. Solsona, "Output admittance synthesizer for synchronverters," *IEEE Trans. Ind. Electron.*, early access, May 25, 2021, doi: 10.1109/TIE.2021.3082069.

[8] I. Cvetkovic, D. Boroyevich, R. Burgos, C. Li, and P. Mattavelli, "Modeling and control of grid-connected voltage-source converters emulating isotropic and anisotropic synchronous machines," in *Proc. IEEE 16th Workshop Control Modeling Power Electron. (COMPEL)*, Vancouver, BC, Canada, Jul. 2015, pp. 1–5.

[9] S. Dong and Y. C. Chen, "Adjusting synchronverter dynamic response speed via damping correction loop," *IEEE Trans. Energy Convers.*, vol. 32, no. 2, pp. 608–619, Jun. 2017.

[10] S. Dong, Y. Chi, and Y. Li, "Active voltage feedback control for hybrid multiterminal HVDC system adopting improved synchronverters," *IEEE Trans. Power Del.*, vol. 31, no. 2, pp. 445–455, Apr. 2016.

[11] J. Driesen and K. Visscher, "Virtual synchronous generators," in *Proc. IEEE Convers. Del. Elect. Energy 21st Century Power Energy Soc. General Meeting*, Pittsburgh, PA, USA, Jul. 2008, pp. 1–3.

[12] J. J. Grainger and W. D. Stevenson, *Power Systems Analysis*. New York, NY, USA: McGraw-Hill, 1994.

[13] P. Kundur, *Power System Stability and Control*. New York, NY, USA: McGraw-Hill, 1994.

[14] Z. Kustanovich, S. Shivratri, H. Yin, and G. Weiss, "Virtual synchronous machines with fast current loops and secondary control," Tech. Rep., 2021.

[15] Z. Kustanovich and G. Weiss, "Synchronverter based photovoltaic inverter," in *Proc. ICSEE*, Eilat, Israel, Dec. 2018, pp. 1–5.

[16] P. Lorenzetti, Z. Kustanovich, S. Shivratri, and G. Weiss, "The equilibrium points and stability of grid-connected synchronverters," *IEEE Trans. Power Syst.*, early access, Jul. 26, 2021, doi: 10.1109/TPWRS.2021.3097954.

[17] F. Mandrile, E. Carpaneto, and R. Bojoi, "Grid-feeding inverter with simplified virtual synchronous compensator providing grid services and grid support," *IEEE Trans. Ind. Appl.*, vol. 57, no. 1, pp. 559–569, Jan. 2021.

[18] F. Mandrile, S. Musumeci, E. Carpaneto, R. Bojoi, T. Dragičević, and F. Blaabjerg, "State-space modeling techniques of emerging grid-connected converters," *Energies*, vol. 13, no. 18, p. 4824, Sep. 2020.

[19] O. Mo, S. D'Arco, and J. A. Suul, "Evaluation of virtual synchronous machines with dynamic or quasi-stationary machine models," *IEEE Trans. Ind. Electron.*, vol. 64, no. 7, pp. 5952–5962, Jul. 2017.

[20] V. Natarajan and G. Weiss, "Synchronverters with better stability due to virtual inductors, virtual capacitors, and anti-windup," *IEEE Trans. Ind. Electron.*, vol. 64, no. 7, pp. 5994–6004, Jul. 2017.

[21] V. Natarajan and G. Weiss, "Almost global asymptotic stability of a grid-connected synchronous generator," *Math. Control, Signals, Syst.*, vol. 30, no. 2, pp. 1–43, Jun. 2018.

[22] J. Roldan-Perez, A. Rodriguez-Cabero, and M. Prodanovic, "Parallel current-controlled synchronverters for voltage and frequency regulation in weak grids," in *Proc. 9th Int. IET Conf. Power Electron., Mach. Drives (PEMD)*, Liverpool, U.K., Apr. 2018.

[23] J. Roldan-Perez, A. Rodriguez-Cabero, and M. Prodanovic, "Design and analysis of virtual synchronous machines in inductive and resistive weak grids," *IEEE Trans. Energy Convers.*, vol. 34, no. 4, pp. 1818–1828, Dec. 2019.

[24] R. Rosso, S. Engelken, and M. Liserre, "Robust stability analysis of synchronverters operating in parallel," *IEEE Trans. Power Electron.*, vol. 34, no. 11, pp. 11309–11319, Nov. 2019.

[25] T. Shao, P. Jia, P. Zheng, T. Q. Zheng, J. Wang, H. Li, M. Liang, and X. Zhang, "A robust power regulation controller to enhance dynamic performance of voltage source converters," *IEEE Trans. Power Electron.*, vol. 34, no. 12, pp. 12407–12422, Dec. 2019.

[26] S. Shivratri, Z. Kustanovich, G. Weiss, and B. Shani, "Virtual synchronous machines with fast current loop," *IFAC-PapersOnLine*, vol. 53, no. 2, pp. 12422–12428, 2020.

[27] Z. Shuai, W. Huang, Z. J. Shen, A. Luo, and Z. Tian, "Active power oscillation and suppression techniques between two parallel synchronverters during load fluctuations," *IEEE Trans. Power Electron.*, vol. 35, no. 4, pp. 4127–4142, Apr. 2020.

[28] A. Tayyebi, D. Groß, A. Anta, F. Kupzog, and F. Dörfler, "Frequency stability of synchronous machines and grid-forming power converters," *IEEE J. Emerg. Sel. Topics Power Electron.*, vol. 8, no. 2, pp. 1004–1018, Jun. 2020.

[29] K. R. Vasudevan, V. K. Ramachandaramurthy, T. S. Babu, and A. Pouryekta, "Synchronverter: A comprehensive review of modifications, stability assessment, applications and future perspectives," *IEEE Access*, vol. 8, pp. 131565–131589, 2020.

[30] H. Wu, X. Ruan, D. Yang, X. Chen, W. Zhao, Z. Lv, and Q.-C. Zhong, "Small-signal modeling and parameters design for virtual synchronous generators," *IEEE Trans. Ind. Electron.*, vol. 63, no. 7, pp. 4292–4303, Jul. 2016.

[31] Q.-C. Zhong and T. Hornik, *Control of Power Inverters in Renewable Energy and Smart Grid Integration*. Chichester, U.K.: Wiley, 2013.

[32] Q.-C. Zhong, G. C. Konstantopoulos, B. Ren, and M. Krstic, "Improved synchronverters with bounded frequency and voltage for smart grid integration," *IEEE Trans. Smart Grid*, vol. 9, no. 2, pp. 786–796, Mar. 2018.

[33] Q.-C. Zhong, P.-L. Nguyen, Z. Ma, and W. Sheng, "Self-synchronized synchronverters: Inverters without a dedicated synchronization unit," *IEEE Trans. Power Electron.*, vol. 29, no. 2, pp. 617–630, Feb. 2014.

[34] Q.-C. Zhong and G. Weiss, "Static synchronous generators for distributed generation and renewable energy," in *Proc. IEEE/PES Power Syst. Conf. Expo. (PSCE)*, Washington, DC, USA, Mar. 2009, pp. 1–6.

[35] Q.-C. Zhong and G. Weiss, "Synchronverters: Inverters that mimic synchronous generators," *IEEE Trans. Ind. Electron.*, vol. 58, no. 4, pp. 1259–1267, Apr. 2011.

ZEEV KUSTANOVICH received the B.Sc. degree in electrical engineering from Ben-Gurion University of the Negev, Be'er Sheva, Israel, in 1997, and the M.Sc. degree in electrical engineering from Technion—Israel Institute of Technology, Haifa, Israel, in 2003. He is currently pursuing the Ph.D. degree with the Power Electronics for Renewable Energy Group, Tel Aviv University, Israel. Since 2003, he has been a Senior Electrical Engineer with Israel Electricity Company. His main research interests include power systems, renewable energy, control theory, and applications to power system stability.

FLORIAN REISSNER received the B.Sc. and M.Sc. degrees from the Technical University of Berlin, Germany, in 2015. He is currently pursuing the Ph.D. degree with the Power Electronics for Renewable Energy Group, Tel Aviv University. From 2015 to 2020, he worked in project management with Vinci Energies, Lyon, and an Innovation Consultant with incubators in Frankfurt and Berlin. In 2020, he started working as an Early Stage Researcher with the Power Electronics for Renewable Energy Group, Tel Aviv University. His current research interests include control techniques in power systems and control theory.

SHIVPRASAD SHIVRATRI received the B.Sc. degree in electrical and electronics engineering from Tel Aviv University, Israel, in 2018, and the M.Sc. degree from the Power Electronics for Renewable Energy Group, Tel Aviv University, in June 2021. His research interests include control theory and its application to power systems.

GEORGE WEISS received the M.Eng. degree in control engineering from the Polytechnic Institute of Bucharest, Romania, in 1981, and the Ph.D. degree in applied mathematics from Weizmann Institute, Rehovot, Israel, in 1989. He was with Brown University, Providence, RI, USA; Virginia Tech, Blacksburg, VA, USA; Ben-Gurion University of the Negev, Be'er Sheva, Israel; the University of Exeter, U.K.; and Imperial College London, U.K. He is currently leading research projects of the European Commission and Israeli Ministry of Energy. His current research interests include distributed parameter systems, operator semigroups, passive and conservative systems, such as linear and nonlinear, power electronics, microgrids, repetitive control, sampled data systems, and wind-driven power generators.